Observation of ballistic carrier propagation in Bi and W by scanning electron microscopy

S. Knauth,[a] J. Lenzner, H. Herrnberger, and W. Grill
Institut für Experimentelle Physik II der Universität Leipzig, Linnéstrasse 5, D-04103 Leipzig, Germany

A. Böhm, A. Gröger, J. Heil,[b] M. Primke,[c] and P. Wyder
Hochfeld-Magnetlabor, Max-Planck-Institut für Festkörperforschung and Centre National de la Recherche Scientifique, B.P. 166, 25 Avenue des Martyrs, F-38042, Grenoble Cedex 9, France

(Received 3 August 1998; accepted for publication 25 September 1998)

A scanning electron microscope with cryogenic sample holder has been employed for spatially resolved excitation of carriers. A point contact at a fixed position on the sample surface opposing the area scanned by the electron beam serves as a local current probe. Ballistic propagation and focusing of electron beam excited carriers is observed in single crystalline high purity samples of bismuth and tungsten over distances of typically 100 μm. Signal contributions from diffusive carrier flow as well as ballistic phonons are observed in addition to the ballistic electron signals. © *1999 American Institute of Physics.* [S0021-8979(99)03301-0]

I. INTRODUCTION

At room temperature the dominating scattering mechanism for electrons in metals is the electron–phonon interaction. This leads to a very short mean free path l^* of the carriers in the range of some nanometers only. Transport is diffusive and is described by Ohm's law when the mean free path is small compared to the samples dimensions. The electron–phonon interaction is approximately proportional to the temperature and can therefore be suppressed by cooling the sample to low temperatures. Below typically 4 K, for metals and semimetals the temperature independent impurity scattering is the dominating scattering mechanism.

If one reduces scattering due to impurities of a sample by carefully preparing very pure single-crystal samples of metals or semimetals, the mean free path l^* can reach values of several hundred μm and can be comparable or larger than the typical sample size. In this case it is possible to observe ballistic propagation of carriers.[1–3] Under these conditions the transport properties reflect the anisotropy of the Fermi surface (FS) and show striking deviations from the diffusive behavior.

Within the semiclassical theory of the dynamics of electrons the group velocity $\mathbf{v}_{gr}$ is related to the wavevector $\mathbf{k}$ by

$$\mathbf{v}_{gr}(\mathbf{k}) = \hbar^{-1} \cdot \nabla_k E(\mathbf{k}). \tag{1.1}$$

Equation (1.1) states that the group velocity is always directed along the gradient of the band structure $E(\mathbf{k})$ and is therefore perpendicular to surfaces of constant energy. Thus the group velocity vectors of electrons at the Fermi energy E_F are perpendicular to the FS.

In the case of free electrons in a paraboloidal band $E(\mathbf{k}) \propto \mathbf{k}^2$ the surfaces of constant energy are spheres and the density of states is equal for all directions of $\mathbf{k}$ and the transport is fully isotropic. The FS of real metals differs considerably from the free electron FS. If directions with vanishing FS curvature exist, the electron current density exhibits singularities in these directions. This highly anisotropic transport phenomenon is called electron focusing (EF).[4]

The surfaces of constant elastic energy in crystals are nonspherical as well, so phonon transport is anisotropic, also. This leads to the well known phonon focusing[5,6] which has been demonstrated in numerous experiments.[7–10] The observation of real space resolved EF has recently been demonstrated[11,12] using light or a point contact for carrier excitation. In this article we present for the first time the observation of EF employing the electron beam of a scanning electron microscope (SEM) for carrier excitation.

II. EXPERIMENT

The excitation of carriers with an electron beam is dominated by local heating. The electron beam penetrates the sample surface and excites a volume which can approximately be described as a sphere with the diameter r_x. Since low temperature scanning electron microscopy is a well established technique and comparable arrangements have been used among others for phonon focusing experiments,[9] we will only point out some results to give an estimate about the range of penetration (r_x) of the primary electrons. A description of this process can be found in the literature.[13] The electrons are deflected by the target atoms by elastic and inelastic collisions. Elastic collisions alter the direction of the primary electrons, inelastic collisions mainly ionize atoms or excite conduction electrons. Inelastic scattering typically occurs with energy transfer in the range of 5–50 eV. This energy loss leads to a relatively well defined path length $r_{\max}$ of the primary electrons which is for light atoms comparable to r_x since the scattering angles are small.

For the heavier nuclei with $Z > 50$ the scattering angles are not small and the electron path resembles the movement

[a]Electronic mail: knauth@physik.uni-leipzig.de
[b]Current address: Leica Microsystems, Postfach 20 40, D-35530 Wetzlar, Germany.
[c]Current address: CTSE-SAP Hewlett-Packard GmbH, Herrenberger-Straße 130, D-71034 Böblingen, Germany.

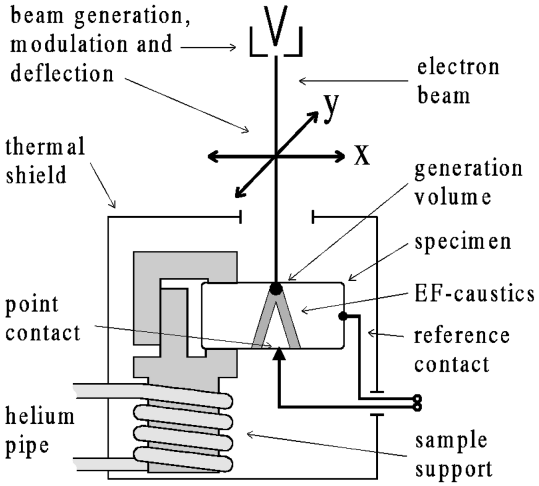

FIG. 1. Scheme of the setup for imaging of ballistic carriers in a metallic single crystal. The carriers are excited in the sample by an electron beam of a SEM. After having traversed the crystal they generate a characteristic potential pattern on the opposite surface which is detected with a stationary point contact.

of a gas particle in kinetic gas theory. Therefore the range of penetration r_x can be shorter by a factor of 2 to 3 than $r_{\max}$ at typical electron beam energies of 15 keV. Since it is observed that r_x is independent of the nuclei charge number it can usually be described by $r_x\rho \propto E^{\mathbf{K}}$ with a parameter K being in the range of 1.3 to 1.7, ρ is the density of the material and E is the electron energy in keV given as unitless number.

For an electron energy $E_{el}=5$ kV we used the empirical relation $r_x\rho = 9.0E^{1,5}\,[\mu\ \mathrm{g\ cm^{-2}}]$ introduced by Cosslett[14] to calculate r_x. For $E_{\mathrm{el}}=20$ kV we used the relation $r_x\rho = 10E^{1,43}\,[\mu\ \mathrm{g\ cm^{-2}}]$ introduced by Drescher.[15] For Bi the value is $r_x=100$ nm for $E_{\mathrm{el}}=5$ keV and $r_x=400$ nm at $E_{\mathrm{el}}=20$ keV, for W the respective values are 200 and 800 nm.

If any electron focusing occurs, the resolution concerning the observed focusing pattern is limited by the width of the radial temperature profile centered in the generation volume. This is in the range of r_x. Therefore the excited volume is an order of magnitude smaller than in experiments with light induced carrier generation. The current injected into the sample by the electron beam is typically 20 nA. This is far too low to explain the signal levels observed in our experiments, since the typical currents needed to generate such signals are known from point contact experiments to be in the mA range. Therefore we expect the signal generating mechanism to be mainly a thermoelectric one like in light induced experiments on electron focusing and the main effect of the beam electrons is just heating. However some measurements show characteristic differences.

Figure 1 shows the experimental setup employed for imaging of electron focusing patterns with the SEM. The sample is mounted in thermal contact with a ^{4}He flow cryostat. The cryostat is equipped with a heater. The temperature can be stabilized at any temperature between 5 and 150 K to about 0.1 K. A thermal shield surrounds the sample. The setup is positioned in the sample chamber of a ComScan CS44 Type SEM. The upper sample surface can be scanned

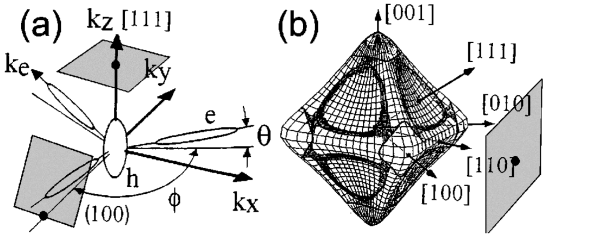

FIG. 2. (a) Fermi surface of Bi (Ref. 16) (e: electrons, h: holes, $\phi=120°$, $\theta\approx 6°$, the size of the pockets is exaggerated with respect to their distance). (b) hole Fermi surface of W, calculated with the data of Ref. 19. Regions with Gaussian curvature lower than 2×10^{-21} m^2 are shaded (Ref. 12). The orientation of the detection planes used for the measurements presented in Figs. 3 and 4 is indicated by the gray rectangles.

with the electron beam through a hole in the thermal shield. A point contact is placed on the opposite sample surface in the center of the area to be scanned. This is done by spot-welding a thin, electrochemically sharpened pin manufactured from copper or tungsten to the sample. The electrical potential between the point contact and a reference contact, which is connected to the edge of the sample, is measured as a function of the beam position. The electron beam intensity is modulated with a frequency $f\approx 100$ Hz and the signal is detected by a lock-in technique. The images of the potential pattern are computer generated using the detected voltage as brightness. Under the assumption of a homogeneous sample crystal, scanning the carrier source instead of the detector only inverts the coordinates with respect to the situation of fixed source and scanned detector.

It is also possible to use backscattering or secondary electron images of the sample for adjustment and to identify surface structures or scratches which might be superimposed on the electron focusing pattern.

III. RESULTS

The FS of bismuth is displayed in Fig. 2(a). It consists of three approximately ellipsoid shaped surface pockets at the T point of the Brillouin zone showing the three fold symmetry of the crystal.[20] The almost cylindrical center parts of the ellipsoids lead to a pronounced enhancement of the electron flux in radial direction. Therefore observable ballistic transport is almost completely restricted to propagation directions in three planes vertical to the axes of the cylinders. The Fermi energy is about $E_f\approx 23$ meV and the effective mass is $m^*\approx 0.01m_e$, where m_e is the free electron mass.[16]

Figure 3(a) shows an experimentally obtained electron focusing pattern of a Bi single crystal disk[17] with a thickness $d=45\ \mu$m, orientated with its large surfaces perpendicularly to the trigonal axis. The image frame is $(110\ \mu\mathrm{m})^2$. The experimental parameters are $U_{\mathrm{el}}=5$ kV and $I_{\mathrm{el}}=22$ nA where U_{el} is the electron beam acceleration voltage and I_{el} is the electron beam current at the sample. The measurement was performed at a temperature of $T=6$ K. The three bright lines result from electrons of the three Fermi ellipsoids. EF occurs in planes perpendicular to k_e due to the small curvature in this direction. The three EF lines do not intersect in one point because of the small tilt of k_e against the (k_xk_y) plane.

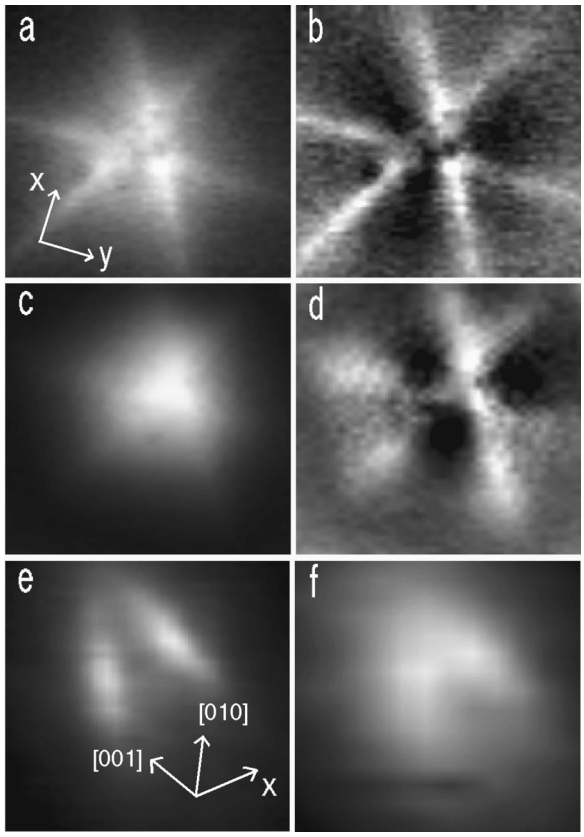

FIG. 3. Electron focusing patterns of two different Bi single crystal slabs. (a)–(d): The observation plane is the k_z-plane (111), crystal thickness $d=45$ μm, image frame $\approx(110\ \mu\text{m})^2$, acceleration voltage $U_{\text{el}}=5$ kV, beam current $I_{\text{el}}=22$ nA. (a) Sample temperature $T=6$ K, (c) $T=15$ K, (a) and (c) show the measured data, (b) and (d) have been created by subtracting a Gaussian profile, which models the diffusive part of the signal, from (a) and (c). (e) and (f): The observation plane is (100), crystal thickness $d=300$ μm, image frame $\approx(1150\ \mu\text{m})^2$, $U_{\text{el}}=20$kV, $I_{\text{el}}=35$ nA. (e) $T=6$ K, (f) $T=7$ K.

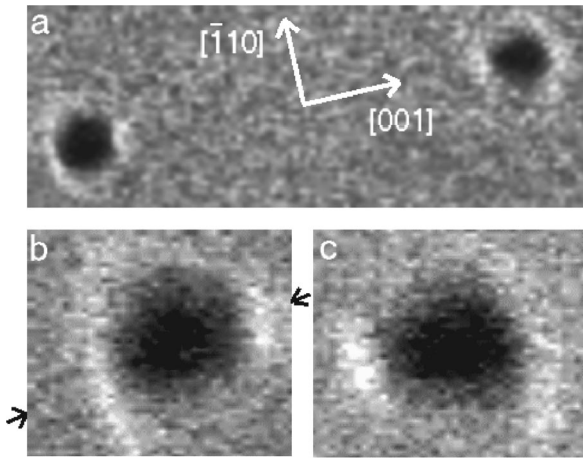

FIG. 4. (a) Electron focusing pattern of a *W* single crystal slab in the (110) plane. Crystal thickness $d=120$ μm, $U_{\text{el}}=20$ kV, $I_{\text{el}}=25$ nA, $T=5.5$ K. Image frame (top) 210 μm$\times$75 μm. (b) and (c) are more detailed images of the two caustics in (a), the image sizes are 40 μm$\times$35 μm each. The two arrows indicate the position of the linescan shown in Fig. 5.

Part of the electrons apparently suffer from multiple scattering processes. These scattered electrons create a rotationally symmetric potential distribution on the sample surface. The focusing pattern is superimposed onto this diffusive signal part. At higher temperatures the diffusive signal dominates the image. Figure 3(c) shows an image of the same Bi sample as in Fig. 3(a), but now measured at $T=15$ K. At this temperature the focusing pattern shows low contrast. The diffusive part of the signal has been modeled by a Gaussian distribution $V(r)$ described by

$$V(\mathbf{r})=V_0 e^{-(\mathbf{r}-\mathbf{r}_0)^2/d^2}, \tag{3.1}$$

where $\mathbf{r}$ and $\mathbf{r_0}$ lie in the observation plane and d is the sample thickness. Figures 3(b) and 3(d) have been computed by fitting Eq. (3.1) to the measurement and subtracting it from the data. In Fig. 3(b) the three focusing lines are dominating the image.

In the center of the image three dark structures outside the inner triangle are visible. These have also been reported[11] in light induced electron focusing measurements on Bi crystals. They are believed to be the contribution of slow transverse phonons. The phonons heat up the sample surface and produce a thermal gradient in the PC. They drag carriers from the hot spot towards and through the PC (phonon drag). These effects generate a thermoelectric voltage at the Bi–Cu point contact.

In the differential image [Fig. 3(d)] the focusing pattern can still be recognized at $T=15$ K. The dark regions which belong to phonons now dominate the images because their propagation conditions do not change significantly between 6 and 15 K while the propagation of ballistic electrons is nearly supressed at the higher temperature.

Figures 3(e) and 3(f) show EF images of another Bi single crystal.[17] The experimental parameters are $U_{\text{el}}=20$ kV and $I_{\text{el}}=35$ nA. The measurement was performed at $T=6$K for image (a) and at $T=7$ K for image (b). In these images the sample surfaces lie in the (100) plane of the crystal. Therefore only two of the focusing planes cross the surface while the third one is orientated nearly parallel to the surface. Image (e) shows ballistic transport, while in image (f) diffusive transport dominates. The onset of the diffusive part occurs within a temperature interval of approximately 1 K.

Figure 4 shows the electron beam induced electron focusing pattern of a tungsten single crystal disk[18] on the (110) surface. The sample thickness is 120 μm. The experimental parameters are $U_{\text{el}}=20$ kV and $I_{\text{el}}=25$ nA. The measurement was performed at $T=5.5$ K. The bright caustic which surround the two dark spots are produced by states of the so-called hole octahedron of the Fermi surface [Fig. 2(b)]. The dark region inside the bright caustic has also been observed for light induced excitation at $T=1.5$ K under otherwise similar conditions,[12] but the negative signal part was far less pronounced than in the measurements presented here. Figure 5 shows a linescan through the center of the triangular focusing structure [Fig. 4(b)] of the tungsten sample used for the measurement demonstrated in Fig. 4. This linescan may be used to estimate the obtainable resolution. The width of the finest detail on this curve is about 5 μm. This sets only an upper limit to the resolution obtainable with the detection scheme presented here. The width of the observed structure may still be a property of the EF in tungsten. The contact

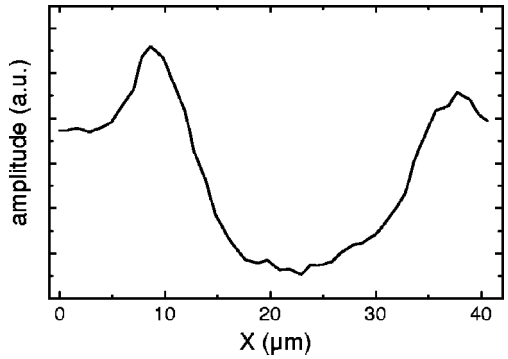

FIG. 5. Linescan through the center of the triangular focusing structure of tungsten. The position of the linescan is marked by the arrows in in Fig. 4(b).

area of the point contact is known to be in the submicron range from its electrical resistance, so we may neglect its influence on the spatial resolving power of the measurements. Thus, Fig. 5 demonstrates that the diameter of the volume in which most of the carriers are excited is at least smaller than 5 μm.

IV. CONCLUSION

We have demonstrated real space resolved detection of electron focusing in metals and semimetals using an electron beam for carrier generation. While the Bi measurements are in quite good agreement to previously published results obtained by light induced electron focusing experiments,[11] the dark structures in W[12] are much more pronounced when measured by the electron beam technique. They are not yet explained satisfactorily for both methods.

The electron beam induced electron focusing detection scheme allows simultaneous observation of EF and of the sample surface by conventional SEM. Surface structures interfering with the EF image can be easily recognized and eliminated.

The method has the potential of high resolution in the range r_x of the generation volume which can be 500 nm or less depending on the sample material and the electron energy of the beam. This offers the possibility of investigating microscopic transport properties in real space of lower quality material classes with a mean free path l^* in the μm range.

[1] Yu. V. Sharvin, L. M. Fisher, Zh. Eksp. Teor. Fiz. Pis'ma Red. **1**, 54 (1965); JETP Lett. **1**, 152 (1965).
[2] V. S. Tsoi, Zh. Eksp. Teor. Fiz. Pis'ma Red. **19**, 114 (1974); JETP Lett. **19**, 70 (1974).
[3] V. S. Tsoi, J. Bass, and P. Wyder, Adv. Phys. **41**, 365 (1992).
[4] A. M. Kosevich, Sov. J. Low Temp. Phys. **11**, 611 (1985).
[5] F. Rösch and O. Weiss, Z. Phys. B **25**, 101 (1976).
[6] A. G. Every, Phys. Rev. B **34**, 2852 (1986).
[7] B. Taylor, H. J. Maris, and C. Elbaum, Phys. Rev. B **3**, 1462 (1971).
[8] G. A. Northrop and J. P. Wolfe, Phys. Rev. Lett. **43**, 1424 (1979).
[9] R. Eichele, R. P. Huebener, and H. Seifert, Z. Phys. B Condens. Matter **48**, 89 (1982).
[10] R. L. Weaver, M. R. Hauser, and J. P. Wolfe, Z. Phys. B **90**, 27 (1993).
[11] J. Heil, M. Primke, K. U. Würz, and P. Wyder, Phys. Rev. Lett. **74**, 146 (1995).
[12] J. Heil, *et al.*, Phys. Rev. B **54**, R2280 (1996).
[13] J. I. Goldstein and H. Yakowitz, *Practical Scanning Electron Microscopy* (Plenum, New York, 1975); L. Reimer and G. Pfefferkorn, *Raster-Elektronenmikroskopie* (Springer, Berlin, 1973).
[14] V. E. Cosslett and R. N. Thomas, Br. J. Appl. Phys. **15**, 1283 (1964).
[15] H. Drescher, L. Reimer, and H. Seidel, Z. Angew. Phys. **29**, 331 (1970).
[16] V. S. Edelman, Adv. Phys. **25**, 555 (1976).
[17] H. Bender and E. Schönherr, Max-Planck-Institut für Festkörperforschung, Heisenbergstraße 1, D-70569 Stuttgart, Germany.
[18] J. Major, P. Keppler, Max-Planck-Institut für Metallforschung, Institut für Physik, Heisenbergstraße 1, D-70569 Stuttgart, Germany.
[19] D. A. Papaconstantopoulos, *Handbook of the Band Structure of Elemental Solids*, Plenum, New York (1986).
[20] E. Fawcett, R. Griessen, W. Joss, and W. Kress, in *Metals: Phonon States and Electron States and Fermi Surfaces*, edited by K. H. Hellwege and J. L. Olsen, Landolt-Börnstein, New Series, Group 3, Vol. 13, Pt. b (Springer, Berlin, 1983); A. P. Cracknell, in *Electron States and Fermi Surfaces of Elements*, edited by K. H. Hellwege and J. L. Olsen, Landolt-Börnstein, New Series, Group 3, Vol. 13, Pt. c (Springer, Berlin, 1984).